Design and multiphysics analysis of a 176 MHz continuous-wave radio-frequency quadrupole

S. V. Kutsaev,* B. Mustapha, P. N. Ostroumov, and A. Barcikowski
ANL, Argonne, Illinois 60439, USA

D. Schrage
TechSource, Los Alamos, New Mexico 87544, USA

J. Rodnizki and D. Berkovits
Soreq NRC, Yavne 81800, Israel
(Received 24 February 2014; published 21 July 2014)

We have developed a new design for a 176 MHz cw radio-frequency quadrupole (RFQ) for the SARAF upgrade project. At this frequency, the proposed design is a conventional four-vane structure. The main design goals are to provide the highest possible shunt impedance while limiting the required rf power to about 120 kW for reliable cw operation, and the length to about 4 meters. If built as designed, the proposed RFQ will be the first four-vane cw RFQ built as a single cavity (no resonant coupling required) that does not require π-mode stabilizing loops or dipole rods. For this, we rely on very detailed 3D simulations of all aspects of the structure and the level of machining precision achieved on the recently developed ATLAS upgrade RFQ. A full 3D model of the structure including vane modulation was developed. The design was optimized using electromagnetic and multiphysics simulations. Following the choice of the vane type and geometry, the vane undercuts were optimized to produce a flat field along the structure. The final design has good mode separation and should not need dipole rods if built as designed, but their effect was studied in the case of manufacturing errors. The tuners were also designed and optimized to tune the main mode without affecting the field flatness. Following the electromagnetic (EM) design optimization, a multiphysics engineering analysis of the structure was performed. The multiphysics analysis is a coupled electromagnetic, thermal and mechanical analysis. The cooling channels, including their paths and sizes, were optimized based on the limiting temperature and deformation requirements. The frequency sensitivity to the RFQ body and vane cooling water temperatures was carefully studied in order to use it for frequency fine-tuning. Finally, an inductive rf power coupler design based on the ATLAS RFQ coupler was developed and simulated. The EM design optimization was performed using CST MICROWAVE STUDIO and the results were verified using both HFSS and ANSYS. The engineering analysis was performed using HFSS and ANSYS and most of the results were verified using the newly developed CST MULTIPHYSICS package.

DOI: 10.1103/PhysRevSTAB.17.072001 PACS numbers: 29.20.Ej, 44.05.+e

I. INTRODUCTION

Soreq NRC, Israel's national laboratory, is exploring the possibilities of upgrading the existing SARAF linac [1]. One of the potential projects is a radio-frequency quadrupole (RFQ) upgrade in collaboration with Argonne. The design and fabrication procedure are based on the successful development of the ATLAS upgrade RFQ [2]. The main requirements for the proposed RFQ are as follows: 1. Absolutely reliable continuous wave (cw) operation for both proton and deuteron beams; 2. Highest possible shunt impedance while keeping the required rf power around 120 kW; 3. Moderate peak fields to avoid breakdowns and lengthy conditioning of the resonator. In particular, the peak electric fields should be below $1.6 \cdot E_K$ where E_K is the Kilpatrick limiting field. This value is based on reliable ATLAS operations experience; 4. High acceleration efficiency (>97%) for the design beam current of 5 mA; 5. Extremely low beam halo in the longitudinal phase space and no transverse rms emittance growth throughout the RFQ.

Due to the lower output energy and frequency compared to the LEDA [3] and IPHI [4] RFQs, the proposed RFQ is much shorter in wavelength units ($\sim 2.2\lambda$) and will be built as a single resonator cavity, and not divided into resonantly coupled cells. In addition, unlike the PXIE RFQ [5] being built at LBNL, this RFQ is designed without π-mode stabilizing loops (PISLs). Moreover, our detailed 3D simulations show that if built as designed, the RFQ will not even need dipole rods to center the quadrupole mode between the neighboring dipole modes, because it is

*kutsaev@anl.gov

already centered by design. As for the π-mode stabilizing loops, we do not believe they are necessary at all, they could actually be the source of additional problems in a cw RFQ such as multipacting, vacuum and power dissipation issues. We note in particular that the group who invented the PISLs [6] at J-PARC abandoned the idea in their latest RFQ [7], which is not even a cw RFQ.

The success of a cw RFQ and its long-term reliable performance is primarily defined by the fabrication technology. Past experience proved that highly reliable, high duty cycle normal conducting accelerating structures can be built using 100% oxygen-free electronic (OFE) copper and brazed in a high-temperature hydrogen atmosphere furnace. Usually, a brazed copper cavity is an integral vacuum and structural vessel. Water cooling channels are plugged by braze joints; replaceable seals are not required between the water and vacuum spaces. This technology has proven to be extremely successful, as evidenced by the long-term operation of linacs for meson factories, neutron sources, and several other RFQs. Brazed copper resonators usually provide high electric fields and intrinsic quality factors nearly equal to the theoretical values.

The proposed SARAF RFQ will be fabricated from OFE copper. Each part of the RFQ will be machined to the required tolerance of $\sim$25 μm, and the segments brazed in a high-temperature furnace in a hydrogen atmosphere. This technology has been successfully applied to cw RFQs such as the RIA prototype RFQ [8] and the ATLAS upgrade RFQ built at Argonne [2]. The dimensions of the proposed segments are similar to those of the ATLAS upgrade RFQ to ensure that the already proven fabrication technology is directly applied to the SARAF RFQ.

In this paper, we present the electromagnetic and engineering design optimization of a 176 MHz cw RFQ for a proposed SARAF linac upgrade. After describing the selected structure, the electromagnetic design is presented. The multiphysics analysis approach is then described, followed by the design optimization of the RFQ cooling system. Finally, the design and simulations of the rf coupler are presented and discussed.

II. RFQ STRUCTURE AND PARAMETERS

A conventional four-vane structure has been selected for this RFQ as described below. The main advantage of a four-vane structure over a four-rod structure is a significantly lower rf power consumption. Most importantly, the rf current density in a four-vane RFQ is much lower than in a four-rod RFQ due to the relatively larger surface area exposed to the magnetic field [9]. As a result, the four-vane structure is much more suitable for cw operation. The vane profile is based on the ATLAS upgrade RFQ, except that this design is a full vane, not a split coaxial. At 176 MHz, the transverse size of a full-vane structure is manageable and a split-coaxial or window-coupled design would significantly increase the power requirements. The structure is about 4 m long and 45 cm in cross section made into four segments. An exploded view of the 3D engineering model of the RFQ is shown in Fig. 1 and the design parameters are summarized in Table I. The output energy could be increased by applying trapezoidal modulation while keeping the same power and length. The output beam energy is a compromise between the length and cost of the RFQ resonator and the number of required low-beta SC cavities [10].

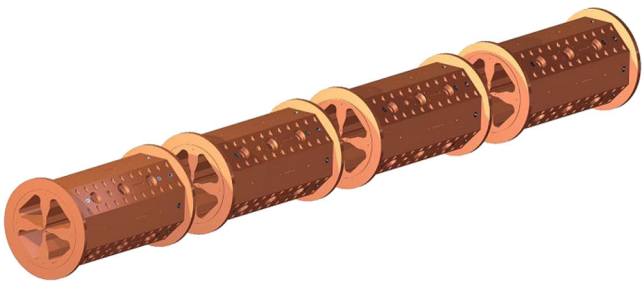

FIG. 1. Detailed 3D engineering model of the RFQ made of four segments.

TABLE I. RFQ design parameters.

Parameter	Value
Lowest q/A	½
Input energy, keV/u	20
Output energy, keV/u	1300
Frequency, MHz	176
Voltage, kV	75
Design current, mA	5
Power, kW	125
Average radius at pole tip, mm	4.4
Maximum modulation factor	2
Minimum transverse phase advance, deg	33
Normalized transverse acceptance, π mm mrad	2.2
Peak surface field, Kilpatrick units	1.6
Number of cells	250

III. ELECTROMAGNETIC DESIGN

The electromagnetic design was mainly developed using CST MICROWAVE STUDIO (MWS) [11] and the final results were verified using HFSS [12] and ANSYS [13]. A full 3D model of the RFQ was built in MWS. Detailed views of the geometry including the vane undercuts and modulations are shown in Fig. 2. In this model, the modulations are sinusoidal along the whole RFQ.

A. Optimization of vane undercuts

In a full-vane structure, vane undercuts are often used to flatten the intervane field along the RFQ by compensating the field depressions at the end walls. These undercuts are applied to both RFQ ends and could in principle be of any geometry [14]. In our case the undercut is of

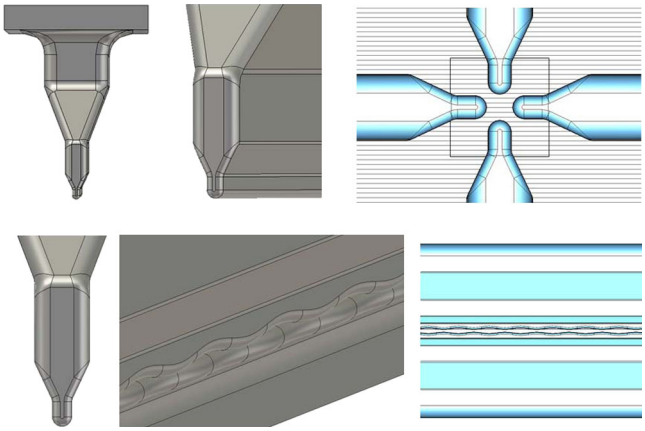

FIG. 2. 3D modeling of the RFQ in MWS.

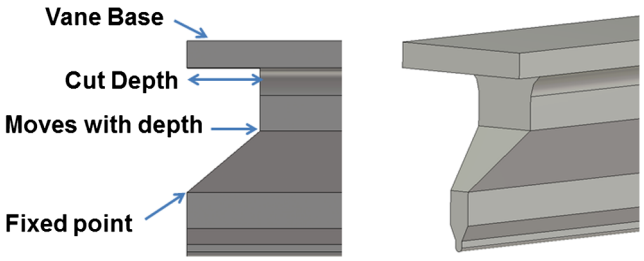

FIG. 3. Geometry of the vane undercut and the vane end after applying the cut.

a trapezoidal shape which is mainly dictated by the vane profile. Figure 3 shows the geometry of the undercut and the vane end after applying the cut. By adjusting the cut depth, the only free parameter, we were able to obtain a flat intervane voltage as shown in Fig. 4. It is worth noting that this optimization was done including vane modulations, which has led to nonsymmetric entrance and exit undercut depths while before applying the modulations the cuts were symmetric.

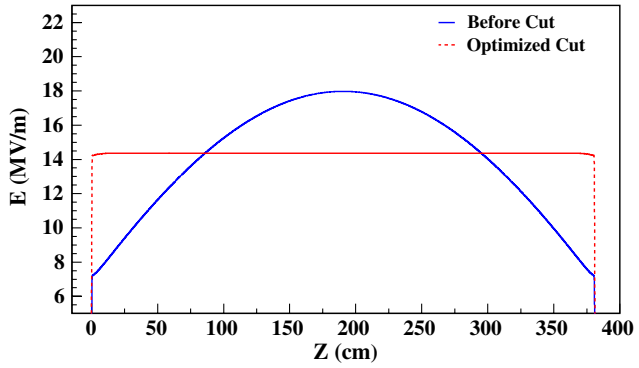

FIG. 4. Intervane field along the RFQ before and after applying the appropriate vane undercuts.

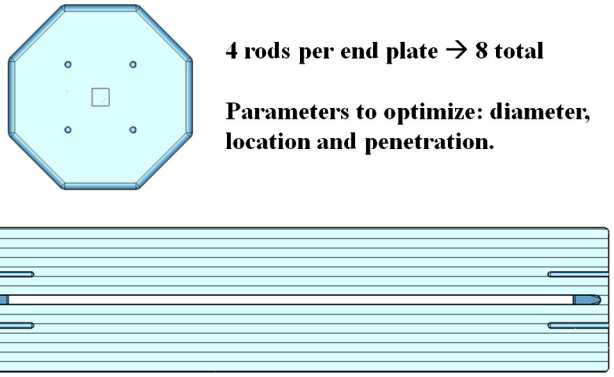

FIG. 5. Number and locations of dipole rods.

B. Mode separation and dipole rods

In order to study the mode separation of the main quadrupole mode from neighboring dipole modes, the electromagnetic (EM) simulation of the full four-segment RFQ model was performed with no symmetry and no modulations. The modulations will only introduce a global shift of the mode frequencies. The results show that the operating mode frequency is centered between two dipole modes with 3 MHz separation from each. This separation is a function of the RFQ length and seems to be ideal for the actual design length [14]. If built as designed this RFQ should not need dipole rods for extra separation, but they may be needed in the case of manufacturing errors. Dipole rods are finger-shaped rods attached to the RFQ end plates, penetrating the rf volume and may require active cooling. Their main purpose is to produce maximum separation of the main mode from neighboring dipole modes by shifting their frequencies. They are located in the quadrupole symmetry planes, as shown in Fig. 5, so they do not affect the quadrupole modes but they are capable of changing the frequency and fields of dipole modes.

The EM simulations showed low sensitivity of the mode separation to variations in the parameters of the dipole rods, namely the diameter, location and penetration. The corresponding results are shown in Fig. 6. We clearly see that the rods introduce a global shift of the dipole mode frequencies which seem to be more sensitive to the location of the rods with respect to the beam axis. The closer to the axis, the more effective the rods are. However, the main mode frequency and field are least affected by the rods when they are at mid-distance between the beam axis and the cavity sidewalls, which is the location of maximal quadrupole symmetry. At this location, the rods have to be 6" deep into the rf volume to see a 0.5 MHz frequency shift of the dipole modes. The frequencies are not very sensitive to the rod diameter but when checking the main quadrupole mode field, a thicker rod disturbs the field more, so a 0.5" rod diameter is near optimal. Based on these studies and considering the manufacturing precision of 25 μm realized on the ATLAS RFQ [2], we may not include dipole rods in the final RFQ design.

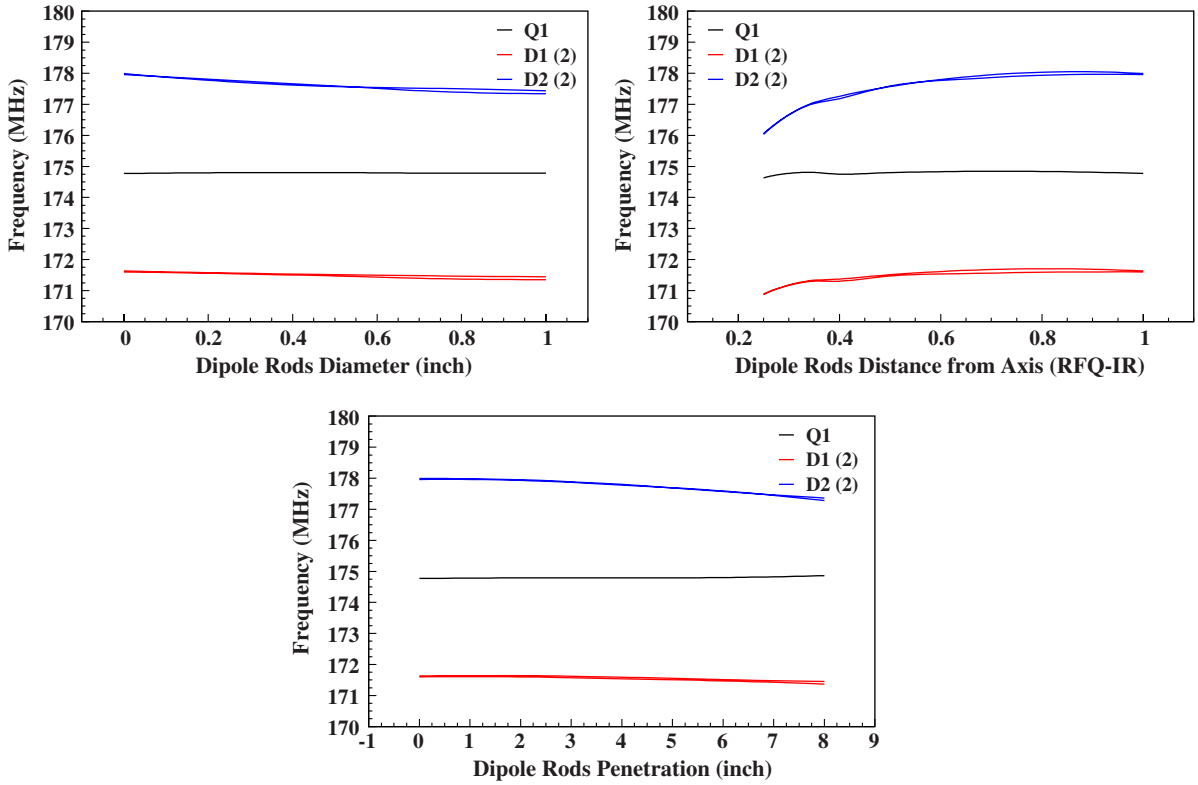

FIG. 6. Effect of dipole rods geometry parameters on mode separation. Q is for a quadrupole mode, D is for a dipole mode and (2) refers to a degenerate mode.

C. Tuners design and simulation

A four-vane RFQ is usually designed and built for a frequency just below the operating frequency to make sure it is tunable to that frequency. For the SARAF RFQ, the design target frequency is 175.4 MHz including all the geometry details. Based on experience with the ATLAS RFQ [15], the simulation error is estimated not to exceed 0.2 MHz. So the tuners should have a range of at least 1 MHz. The RFQ will have two tuners per quadrant per segment making a total of 32 tuners as shown in Fig. 7. The tuner diameter is 2.5" and could go up to 2" deep inside the RFQ volume. Figure 8 shows a comparison of the intervane field between a case where the tuners are uniformly distributed along the RFQ and inserted to the same depth and a case of nonuniform tuning. Only the frequency is tuned in both cases. We notice that in the uniform case, the field flatness is preserved while in the other case, a slope in the intervane field is observed and will require more optimization of the tuners depth to restore the field flatness. Based on these results, we decided to separate the tuner ports from coupling and vacuum ports to allow for uniform tuning that preserves the field flatness. In addition, a uniform distribution of tuners allows more flexibility in tuning both the frequency and field flatness in the case of manufacturing errors leading to a nonflat intervane field. The simulated frequency sensitivity to the tuners is 37.5 kHz per tuner per inch, which is a 2.4 MHz tuning range if all tuners were inserted 2 inches deep into the cavity.

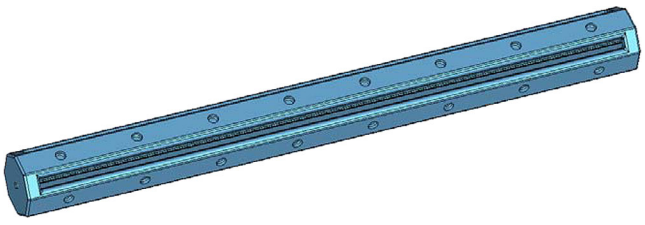

FIG. 7. Full RFQ model showing the location of the tuners.

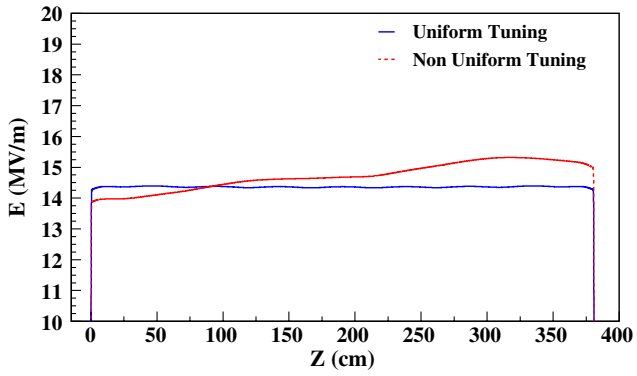

FIG. 8. Uniform and nonuniform tuning effect on the intervane field along the RFQ.

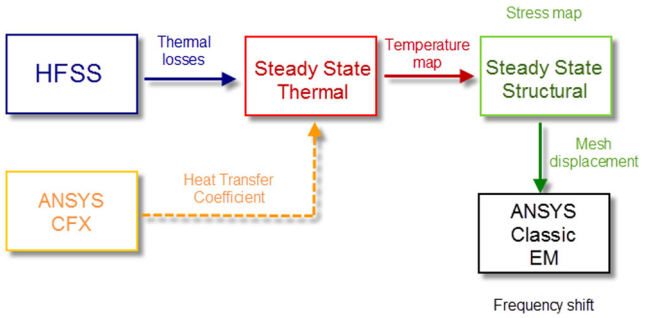

FIG. 9. Multiphysics analysis scheme based on HFSS and ANSYS.

IV. MULTIPHYSICS ANALYSIS APPROACH

The multiphysics analysis is a coupled electromagnetic, thermal and mechanical analysis of the structure. The magnetic field distribution on the copper surface is used to calculate the thermal losses which are loaded to the thermal model. The results of the thermal solution include a temperature map which is used to calculate the structural stresses and deformations. The latter are needed to simulate the resonant frequency shift and field distortions in the RFQ. The HFSS and ANSYS software were used for these simulations and Fig. 9 shows the simulation scheme. In addition to ANSYS, most of the results were verified using the recently developed CST MULTIPHYSICS package.

V. RFQ COOLING SIMULATIONS

The initial cooling system is shown in Fig. 10(a). It consists of eight 0.25" outer tank or body channels and eight 0.375" vane channels per segment. This layout was based on the ATLAS RFQ cooling system [16]. According to this experience, the speed of cooling water was chosen equal to 15 fps. In the simulations, the background

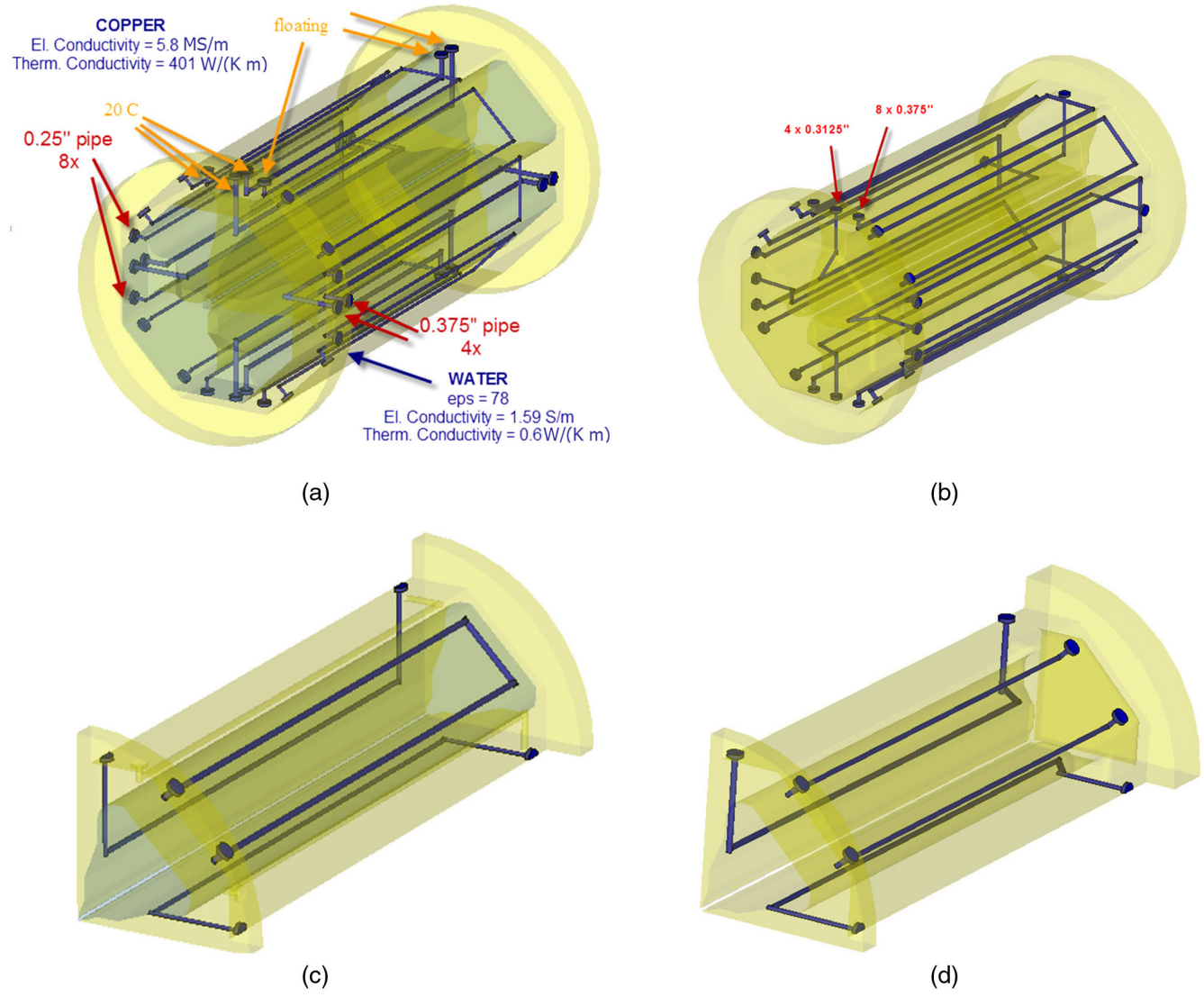

FIG. 10. Iterations of cooling channels.

TABLE II. Input values and results of the analytical calculations of heat transfer coefficients.

Parameter	Value	
Channel type	Vane	Body
Velocity, fps	15	
Pipe diameter, in	0.375	0.25
Fluid density, kg/m^3	998	
Fluid viscosity, N s/m^2	0.001	
Fluid thermal conductivity, W/(m K)	0.58	
Prandtl number	5.7	
Reynolds number	43470	28980
Nusselt number	252.8	182.6
Heat transfer coefficient, kW/(m^{2}K)	16.6	18.0

temperature was considered to be 20 °C and the rf losses were normalized to 75 kV intervane voltage.

A. Benchmarking the simulations

To calculate the heat transfer coefficient of cooling liquid forced convection, it is necessary to know whether the flow is turbulent or laminar. This can be determined by calculating the Reynolds number using the formula below for pipes [17]:

$$\mathrm{Re} = \frac{vD\rho}{\mu}. \tag{1}$$

Here v corresponds to the liquid velocity, D is the pipe diameter, ρ and μ are the liquid density and viscosity respectively. In our case, the Reynolds number is higher than 28000 and clearly indicates a turbulent flow. The Nusselt number, needed to calculate the heat transfer coefficient for the turbulent regime, can be calculated using the Dittus-Boelter correlation,

$$\mathrm{Nu} = 0.023 \cdot \mathrm{Re}^{0.8} \cdot \mathrm{Pr}^{0.4}, \tag{2}$$

where Pr is the Prandtl number. Finally, the heat transfer coefficient is calculated using the expression

$$h = \frac{\lambda}{D}\mathrm{Nu}. \tag{3}$$

For a vane channel, the heat transfer coefficient is 16.6 kW/(m^{2}K) while for a body channel it is 18.0 kW/(m^{2}K). Table II summarizes all the input values and results of the analytical calculations. To verify these

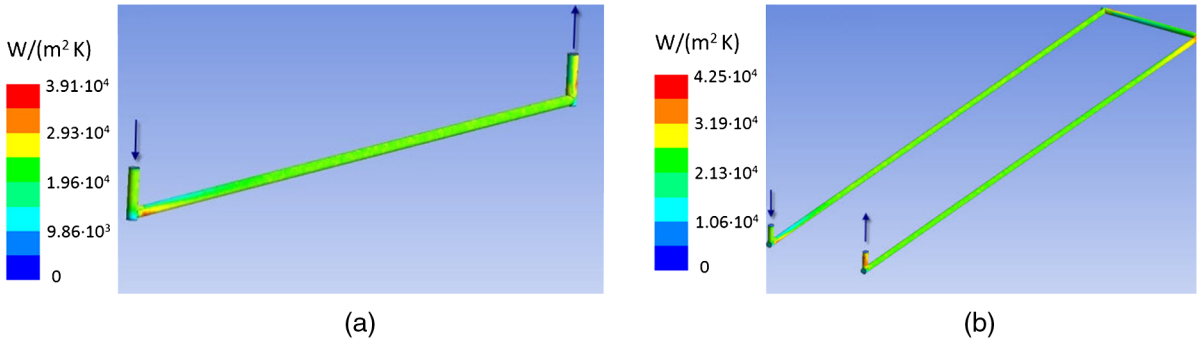

FIG. 11. CFD heat transfer coefficient distribution.

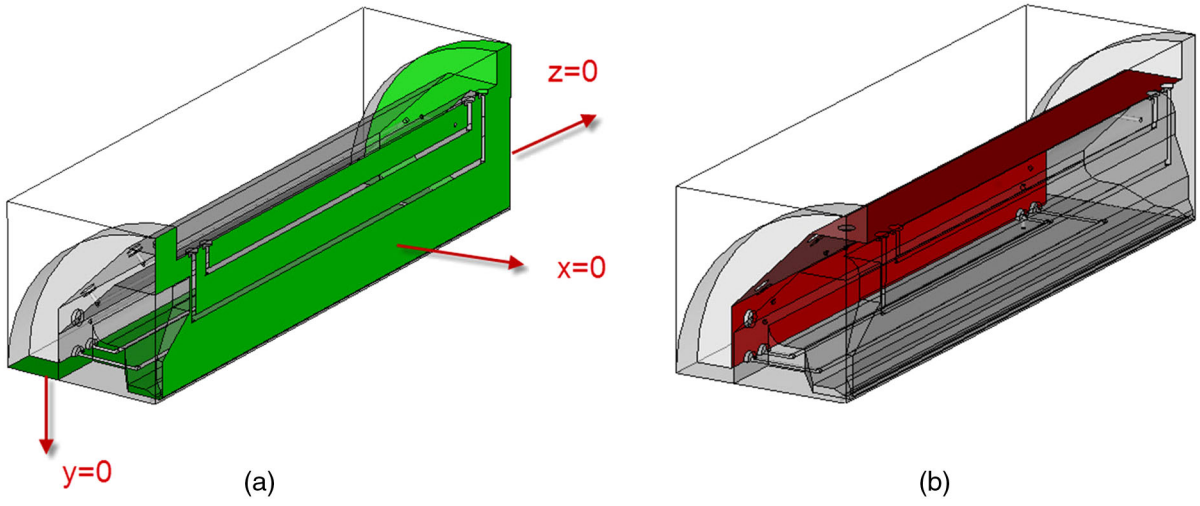

FIG. 12. Structural simulations loads and constrains.

TABLE III. Comparison of the thermal and structural analysis results between ANSYS and CST.

Software	CST	ANSYS
Intervane voltage, kV	75	
Maximal temperature, °C	52.19	51.25
Maximal equivalent stress, MPa	29.1	21.1
Maximal absolute deformation, μm	165.0	163.8
Frequency shift, kHz	Unavailable	−243.0

numbers, the computational fluid dynamics (CFD) program ANSYS CFX was used for direct simulations. Heat transfer coefficient maps for the two different channels can be seen in Fig. 11. Although the distribution is not uniform, the average value agrees with the analytically calculated one. To reduce the CPU time, the analytical value is used instead of the CFD distribution in further simulations.

Thermal and structural analysis for one end section of the RFQ was performed both in CST STUDIO and ANSYS. The results are compared in Table III. In structural simulations, the RFQ section was constrained at one end face and atmospheric pressure applied on the outer walls as shown in Fig. 12. The slight difference in the temperature results can be explained by the different mesh types in the thermal solver. We have also done an additional mesh refinement in ANSYS. Nevertheless, these independent results benchmark each other well.

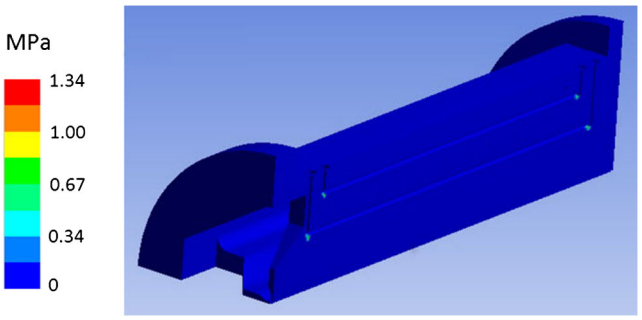

FIG. 13. von Mises stress distribution in an unconstrained model.

TABLE IV. Comparison of the simulated and analytically calculated RFQ analysis results.

	Analytical	Simulated
Ambient temperature, °C	20	
Applied temperature, °C	50	
Maximal equivalent stress, MPa	0	0 (except in ill-formed elements)
Maximal axial deformation, μm	163.0	175.1
Frequency shift, kHz	−30	−31.87

The other approach to benchmark the structural results is to simulate the unconstrained model with a uniform temperature distribution and compare the results to the analytical prediction. It is clear that in the unconstrained model, the von Mises stresses should be equal to zero, but the simulations show that in some areas (see Fig. 13) there are actually some nonzero stresses. This is caused by some ill-formed mesh elements. In addition to being nonphysical, the nonzero stresses are located in the cooling channels, so they can be disregarded. Otherwise, the simulated results are in good agreement with the analytical prediction (Table IV). The ill-formed mesh elements also explain

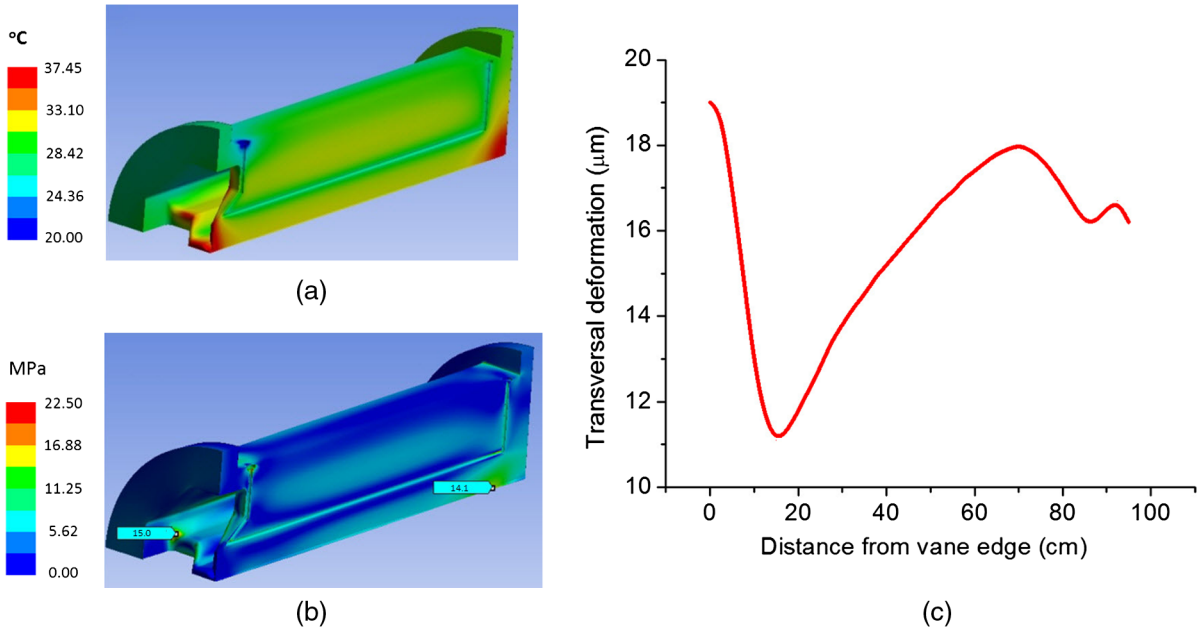

FIG. 14. Results for the final cooling channel configuration.

TABLE V. Iterations of cooling channels configuration and corresponding results.

Cooling channels configuration	Initial	1st revision	2nd revision	Final
Number of vane channels	8	4	4	4
Number of body channels	8 (return)	8 (return)	4 (return)	8 (no return)
Diameter of vane channels	0.375”	0.375”	0.375”	0.3125”
Diameter of body channels	0.25”	0.3125”	0.3125”	0.375”
Maximum temperature (°C)	51.2	40.0	41.3	38.5
Maximum stress (MPa)	21.1	23.0	16.7	12.8
Maximum total deformation (μm)	164	131	182	196
Frequency shift (kHz)	−243	−263	−238	−143

the difference between maximum stresses in CST and ANSYS simulations.

B. Optimization of cooling channels

The simulation results for the initial configuration of cooling channels show a relatively high temperature and stress. In order to reduce the maximum temperature and optimize the cooling system performance, the water channels layout was reorganized in a first revision as shown on Fig. 10(b). According to the results, eight vane channels per segment are excessive so their number was reduced to four. The shape of the pipe was also modified such that it follows the shape of the vane cut. Also, the body channels diameter was increased from 0.25” to 0.3125” to compensate for the reduced heat removal capability.

Further optimization has led to a second revision by the removal of four-body channels per segment from the RFQ sectors where both vane and body channels are present [see Fig. 10(c)]. This modification reduced the maximum stress and the frequency shift but it increased the maximum temperature and total deformation. In addition, fluid dynamics (CFD) simulations showed that the water temperature increase is different in the body and vane channels by 2.4 °C. Both temperature and stress peaks are located on the edges of the vane cut. To reduce them the following modifications were applied, leading to the final cooling system design shown in Fig. 10(d): (i) The RFQ edges blending radius was increased from 0.25” to 0.5” at the vane base and around the flat cut; (ii) The body cooling channels were separated into two independent channels to avoid the reversal flow; (iii) The vane channel diameter was reduced to 0.3125” while the body channel’s was increased to 0.375” to equalize the water output temperature at the same cooling water speed of 15 fps corresponding to a mass flow rate of ∼50 GPM per segment.

After these iterations and a series of thermal and mechanical simulations, we found the best cooling channels configuration that produces an acceptable operating temperature with minimal von Mises stresses, which are at least 3 times less than the yield stress of copper [18], as well as deformation and frequency shift less than 10% of the tuning range. The details and corresponding results for the different iterations are given in Table V. The results are for one end segment. Simulations were also performed for a middle segment and found to be consistent. The final configuration has a total of 12 cooling channels per segment, one per vane and two per quadrant. A quadrant is a side of the octagonal RFQ wall with no vane. Figure 14 shows the temperature map, the von Mises stress map and the transverse vane deformation for the final configuration of the cooling channels.

C. Water flow and fluid dynamics simulations

Fluid dynamics simulations were performed to determine the temperature change of the cooling water between the inlet and outlet of the cooling channels. For these

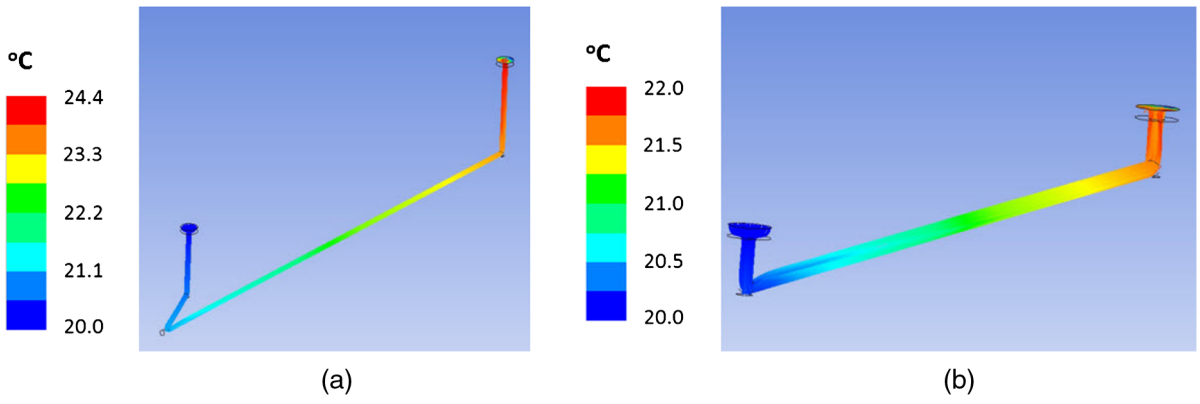

FIG. 15. Results of fluid dynamics simulations showing the water temperature in the cooling channels.

TABLE VI. Effect of channel to inner RFQ surface distance.

Parameter	Value	
Channel offset, mm	5	10
Maximum temperature, °C	38.5	38.0
Maximum stress, MPa	12.8	14.4
Maximum transverse vane-tip deformation, μm	15.7	18.9
Frequency shift, kHz	−142.5	−181.6
Body cooling water temperature rise, °C	2.6	2.6
Vane cooling water temperature rise, °C	3.3	3.3
Power removed, kW	38.2	38.2

simulations, the average thermal flux in the channel is obtained from the thermal solver then integrated over the channel's cross section. The calculated flux is 140.2 kW/m^2 for a vane channel and 92.25 kW/m^2 for a body channel, leading to a 4.24 kW integrated flow for a vane and 2.33 kW for a quadrant, a total of 35.6 kW per segment. The corresponding results are shown in Fig. 15. As mentioned above, based on these results, the final cooling channel diameters were adjusted to match the temperature rise in the vane and body channels. The vane channels are now 0.3125" in diameter while the body channels have 0.375" diameter.

D. Cooling channels to inner surface distance

Another important parameter is how close the cooling channels could be to the inner cavity wall. Obviously the closer the better the cooling performance but there exists a technological limit. The final design was simulated with two different distances of the cooling channels to the inner RFQ surface, the first is 5 mm which is at the manufacturing limit and the second is 10 mm which is a more conservative value. The comparison is given in Table VI. We clearly note that a 10 mm distance does not deteriorate the main output parameters, but in order to further reduce vane deformation and stress, we have adopted the 5 mm case for the final RFQ design.

E. Frequency sensitivity to cooling water temperature

The total frequency shift is a combined effect of cavity radius change and vane tip deformation. The first can be controlled by varying the body cooling water temperature while the second by controlling the vanes cooling water temperature. Therefore, it is possible to use the cooling system to fine-tune the RFQ frequency. Multiphysics simulations with different cooling water temperatures were performed and Fig. 16 shows the frequency response to changing vane and body cooling water temperatures. From the opposite slopes, we note that a zero frequency shift could be achieved either by increasing the body cooling water temperature or by decreasing the vane cooling water temperature. The temperature frequency sensitivities are comparable but of opposite signs. It is +21 kHz/°C for the body temperature and −24 kHz/°C for the vane temperature.

Concluding this section, we have developed a cooling system that provides a reasonable temperature in the operating regime with an equivalent stress 3 times less than the recommended limit [19].

VI. COUPLER DESIGN AND SIMULATIONS

To input rf power into the cavity, an inductive coupler similar to the ATLAS upgrade RFQ coupler, was developed. Figure 17 shows the engineering model of the coupler. The cooling system consists of both water and air cooling. Water cooling is for the inner and outer conductors including the antenna. Like in the RFQ cavity, the

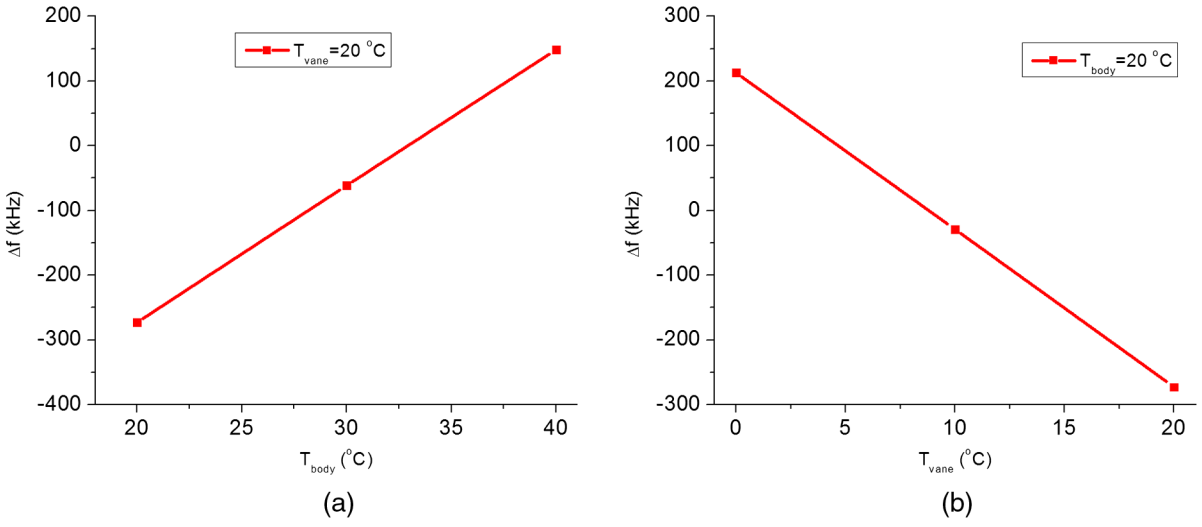

FIG. 16. RFQ frequency response to changing cooling water temperatures.

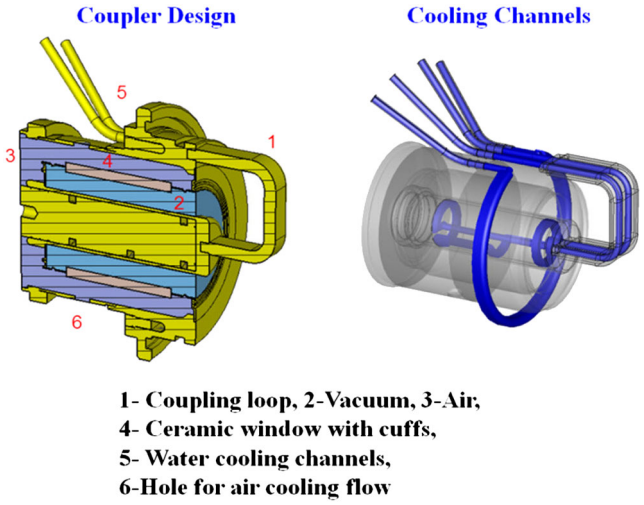

FIG. 17. rf coupler design (left) and cooling channels (right).

water flow speed is 15 fps. Air flow cooling is to reduce the temperature of the ceramic window. The air mass flow rate is 6.3 gpm. The results of CFD simulations of the air flow are shown on Fig. 18. As no structural analysis is required, the electromagnetic and thermal simulations were performed using CST STUDIO, mainly due to its convenience and its reliable frequency domain solver. The simulations assumed a 60 kW rf power going through the coupler at the critical coupling regime achieved by connecting the coupler to the RFQ and appropriately rotating the coupling loop. The results in Fig. 19 show a significant overheating of 218 °C on the steel cuffs. Changing the cuffs material to copper solved this problem and reduced the maximum temperature to 38.3 °C. The technology of brazing copper cuffs directly to the ceramic has been already implemented in the ATLAS RFQ couplers.

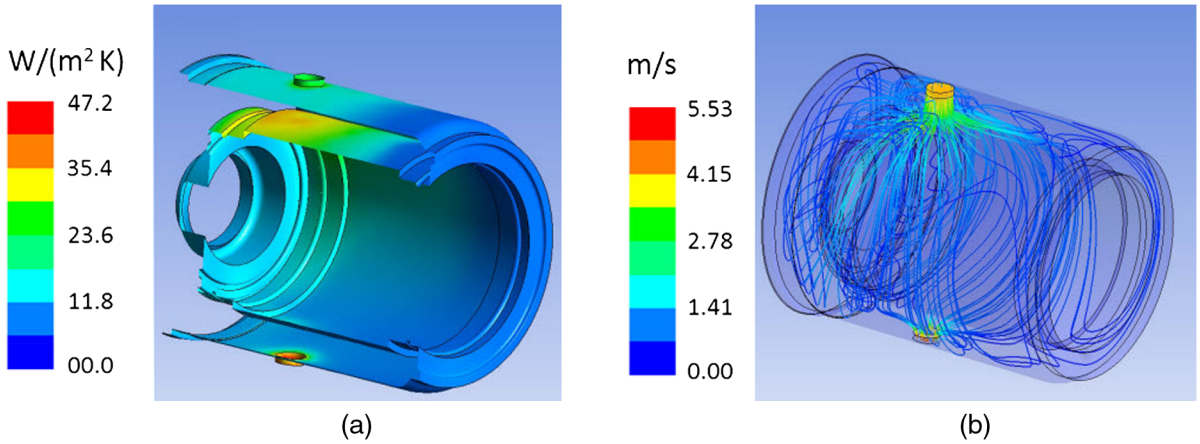

FIG. 18. Results of air cooling simulations from ANSYS.

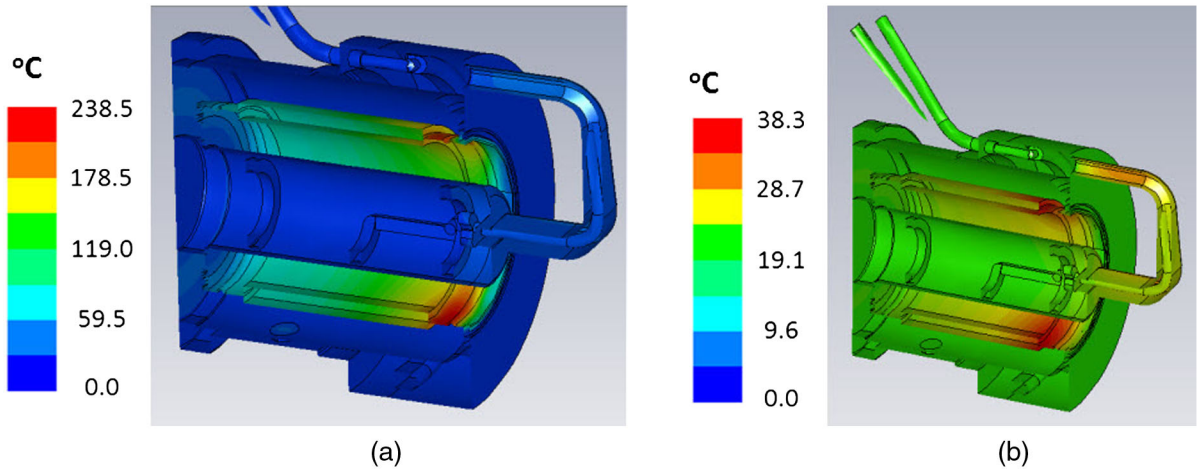

FIG. 19. Results of thermal simulations from CST with steel or copper cuffs.

VII. SUMMARY

We have designed and simulated a 176 MHz cw RFQ. A complete engineering and multiphysics analysis was performed including electromagnetics, thermal and mechanical analysis. The RFQ is a four-vane structure with optimized trapezoidal vane undercuts for flat intervane field. It is about 4 m long subdivided into four segments with good mode separation and will not need dipole rods if built as designed. This RFQ is the first four-vane cw RFQ designed to be built as a single resonator structure, without π-mode stabilizing loops or dipole rods, thanks to well advanced 3D simulation tools and much improved fabrication precision. Based on ATLAS RFQ fabrication technology we expect that the SARAF RFQ will be built per prints with accuracy of ~ 25 μm for critical dimensions. The RFQ has two tuners per quadrant per segment, a total of 32 with a full tuning range of 2.4 MHz. The tuners ports will be separate from the coupling and vacuum ports to allow for uniform tuning with minimal effect on field flatness. The cooling channels were optimized in order to minimize vane deformation and stress. An rf coupler design was developed and simulated as well. The simulation showed that replacing the steel cuffs with copper ones should reduce the temperature significantly. As was successfully implemented in the ATLAS upgrade RFQ, we are planning to design trapezoidal vane modulation which would increase the output energy for the same RFQ power and length. The implementation of trapezoidal modulation will not change any of the RFQ multiphysics properties reported in this paper.

ACKNOWLEDGMENTS

This work was supported by the U.S. Department of Energy, Office of Nuclear Physics, under Contract No. DE-AC02-06CH11357 and ANL WFO No. 85Y47.

[1] D. Berkovits *et al.*, in *Proceedings of the 26th International Linear Accelerator Conference, LINAC-2012, Tel Aviv, Israel* (JACoW, Tel Aviv, Israel, 2012); L. Weissman *et al.*, in *Proceedings of the 25th International Linear Accelerator Conference, LINAC-2010, Tsukuba, Japan* (KEK, Tsukuba, Japan, 2010).

[2] P. N. Ostroumov *et al.*, Phys. Rev. ST Accel. Beams **15**, 110101 (2012).

[3] D. Schrage *et al.*, in *Proceedings of the Particle Accelerator Conference, Vancouver, BC, Canada, 1997* (IEEE, New York, 1997), p. 1093.

[4] O. Piquet *et al.*, *Proceedings of the 10th European Particle Accelerator Conference, Edinburgh, Scotland, 2006* (EPS-AG, Edinburgh, Scotland, 2006), p. 291.

[5] S. P. Virostek *et al.*, in *Proceedings of the 25th Particle Accelerator Conference, PAC-2013, Pasadena, CA, 2013* (IEEE, New York, 2013), p. 1025.

[6] A. Ueno *et al.*, in *Proceedings of the 17th International Linear Accelerator Conference (LINAC-1994), Tsukuba, Japan, 1994* (KEK, Tsukuba, Japan, 1994), p. 166.

[7] Y. Kondo *et al.*, Phys. Rev. ST Accel. Beams **16**, 040102 (2013).

[8] P. N. Ostroumov *et al.*, in *Proceedings of the 23rd International Linac Conference, LINAC-2006, Knoxville, TN, 2006* (JACoW, Knoxville, TN, 2006), p. 767.

[9] T. Wangler, *RF Linear Accelerators* (Wiley-VCH, Weinheim, 2008), 2nd ed.

[10] J. Rodnizki *et al.*, in *Proceedings of the 26th International Linear Accelerator Conference, LINAC-2012, Tel Aviv, Israel* (JACoW, Tel Aviv, Israel, 2012).

[11] CST Simulation packages, http://www.cst.com.

[12] HFSS, http://www.ansys.com/Products/.

[13] ANSYS, http://www.ansys.com.

[14] B. Mustapha, S. V. Kutsaev, and P. N. Ostroumov, in *Proceedings of the 25th Particle Accelerator Conference, PAC-2013, Pasadena, CA, 2013*, Ref. [5], p. 990.

[15] B. Mustapha, A. Kolomiets, and P. Ostroumov, Phys. Rev. ST Accel. Beams **16**, 120101 (2013).

[16] T. Schultheiss *et al.*, in *Proceedings of the 24th Particle Accelerator Conference, PAC-2011, New York, 2011* (IEEE, New York, 2011), p. 1334.

[17] F. Kreith, *The CRC Handbook of Thermal Engineering* (CRC Press, Boca Raton, 2000).

[18] G. Li, B. G. Thomas, and J. F. Stubbins, Metall. Mater. Trans. A **31**, 2491 (2000).

[19] A. M. Howatson, P. G. Lund, and J. D. Todd, *Engineering Tables and Data* (Chapman and Hall, London, 1972).